A Geometric Approach to Segmentation and Analysis of $3D$ Medical Images

R. Malladi,[*] R. Kimmel,[*] D. Adalsteinsson,[*] G. Sapiro,[†] V. Caselles,[‡] J. A. Sethian[§]

Abstract

A geometric scheme for detecting, representing, and measuring $3D$ medical data is presented. The technique is based on deforming $3D$ surfaces, represented via level-sets, towards the medical objects, according to intrinsic geometric measures of the data. The $3D$ medical object is represented as a (weighted) minimal surface in a Riemannian space whose metric is induced from the image. This minimal surface is computed using the level-set methodology for propagating interfaces, combined with a narrow band technique which allows fast implementation. This computation technique automatically handles topological changes. Measurements like volume and area are performed on the surface, exploiting the representation and the high accuracy intrinsic to the algorithm.

Key words: *Deformable models, minimal surfaces, segmentation, measurements, level sets, narrow-band methods, fast implementation.*

1. Introduction

One of the basic problems in medical imaging is to detect the boundaries of the objects of interest, efficiently represent them, and perform measurements significant for diagnosis, surgery, or other applications. Active contours, initially proposed by Kass *et al.*, and deformable surfaces introduced by Terzopoulos *et al* [44], can be used to solve the first part of this goal, i.e. the segmentation task. These models are based on deforming an initial contour or surface towards the boundary of the object to be detected. The deformation is obtained by minimizing a functional designed such that its (local) minima is obtained at the boundary of the object [4, 44].

Implicit surface-evolution models for medical image segmentation were proposed by Caselles *et al.* [5] and by Malladi *et al.* [28, 29]. In these models, the surface propagates by an implicit velocity containing two terms, one related to the regularity of the deforming shape and the other attracting it to the boundary. The model is given by a geometric flow based on mean curvature motion, and is not the result of minimizing an energy functional. At their core, these models rely on the Osher-Sethian level-set model for evolving surfaces [34, 39]. The level-set approach offers a robust, stable, and efficient numerical algorithm that allows for complex changes in topology, accurate evaluation of curvatures, and straightforward implementation. In addition, fast implementations of this approach were introduced by Adalsteinsson and Sethian [1] and Malladi, Sethian, and Vemuri [30]. In the energy based approach, the flexibility in topology can be obtained only if special tracking procedures are implemented [31, 42]. For details about a wide collection of level-set applications, see [40].

In [6], formal mathematical relation between these two approaches for $2D$ object detection is shown, proposing the "geodesic active contours." As shown in [6], the geodesic active contours model has the following main properties:

1. It connects energy and curve evolution approaches of active contours.
2. Presents the snake problem as a geodesic computation.
3. Improves existing models as a result of the geodesic formulation.
4. Allows simultaneous detection of interior and exterior boundaries of several objects without special contour tracking procedures.

[*]Mail Stop: 50A-2152, Lawrence Berkeley National Laboratory, University of California, Berkeley, CA 94720

[†]Hewlett-Packard Labs., 1501 Page Mill Rd., Palo Alto, CA 94304

[‡]Dept. of Mathematics and Informatics, University of Illes Balears, 07071 Palma de Mallorca, Spain

[§]Dept. of Mathematics, University of California, Berkeley, CA 94720

5. Holds formal existence, uniqueness, and stability results.

6. Stops automatically.

The $2D$ model in [6] was then extended to $3D$ surfaces in [7, 8]. The proposed $3D$ approach has the same important properties as its $2D$ analogous one. The original model in Malladi *et al.* [29] (and in [5]) has also been extended to $3D$ and coupled with fast tube methods for approximating interface position in [24, 27]. In this paper, we combine the model in [7], which is revisited here, with the fast numerical approach first described in [1, 30] and extended to $3D$ in [2, 24, 27] and present a complete approach for $3D$ medical data analysis. Then, following the $2D$ analysis started in [36], we exploit the representation and the high accuracy intrinsic to the algorithm to compute important characteristics such as volume and surface area of the segmented $3D$ medical organs.

We should note that the deformable surfaces model used here is related to a number of previously or simultaneously developed results. It is of course closely related to the works of Terzopoulos and colleagues on energy based deformable surfaces, and the works by Malladi *et al.* and Caselles *et al.* [5, 24, 29]. It is an extension of the $2D$ model derived in [6]; see [7, 8]. The basic equations in this paper, as well as the corresponding $2D$ ones in [6], were simultaneously developed in [20, 21, 41]. In [20, 21], the authors base their approach on gradient flows, while in [41], the development partially follows from the Mumford-Shah segmentation technique [32]. Similar $3D$ models are studied in [45, 46] as well. In [43], the authors work with multiple initializations and multiple parameter-space, partially motivated by the shape theory in [22], using the equations in [5, 28, 29]. In this paper, we develop a complete and fast approach for 3D segmentation and area and volumetric measurements on the segmented objects; see Whitaker [46] for fast multi-scale implementation. For more details on the similitude and differences between these approaches, see [6, 7, 8]. The details of tube method for moving $3D$ shapes and a comparison to the traditional full matrix method may be found in [24, 27].

2. Basic approaches of deformable surfaces

The $3D$ deformable surface model was introduced by Terzopoulos *et al.* [44] and further extended by others (e.g. [11, 12, 13]). A parameterized surface $v(r,s) = (x(r,s), y(r,s), z(r,s))$, $(r,s) \in [0,1] \times [0,1]$, is considered, and the energy functional is given by

$$E(v) = \int_\Omega \left[\omega_{10} \left| \frac{\partial v}{\partial r} \right|^2 + \omega_{01} \left| \frac{\partial v}{\partial s} \right|^2 + \omega_{11} \left| \frac{\partial^2 v}{\partial r \partial s} \right|^2 + \omega_{20} \left| \frac{\partial^2 v}{\partial r^2} \right|^2 + \omega_{02} \left| \frac{\partial^2 v}{\partial s^2} \right|^2 + P \right] dr ds,$$

where $P = - \parallel \nabla v \parallel^2$, or any related decreasing function of the gradient. The first terms are related to the smoothness of the surface, while the last one is responsible for attracting it to the object. The evolution of the surface is expressed via Euler-Largange equations. From an initial surface $\mathcal{S}_0$, generally near the desired $3D$ boundary O, the algorithm tries to deform $\mathcal{S}_0$ towards a local minimum of E.

The geometric models proposed in [5, 29] can easily be extended to $3D$ object detection. Let $Q =: [0,a] \times [0,b] \times [0,c]$ and $I : Q \rightarrow^+$ be a given $3D$ data image. Let $g(I) = 1/(1+|\nabla \hat{I}|^p)$, where $\hat{I}$ a regularized version of I, and $p = 1$ or 2. $g(I)$ acts as an edge detector so that the object boundary we are looking for is ideally given by the equation $g = 0$. Our initial active surface $\mathcal{S}_0$ will be embedded as a level-set [34, 39] of a function $u_0 : Q \rightarrow^+$, say $\mathcal{S}_0 = \{x : u_0(x) = 0\}$ with u_0 being positive in the exterior and negative in the interior of $\mathcal{S}_0$. The evolving active surface is defined by $\mathcal{S}_t = \{x : u(t,x) = 0\}$ where $u(t,x)$ is the solution of

$$\begin{aligned} \frac{\partial u}{\partial t} &= g(I)|\nabla u| \mathrm{div}\left(\frac{\nabla u}{|\nabla u|}\right) + \nu g(I)|\nabla u| \\ &= g(I)(\nu + H)|\nabla u|, \end{aligned} \quad (1)$$

with initial condition $u(0,x) = u_0(x)$ and Neumann boundary conditions. Here $H = \mathrm{div}\left(\frac{\nabla u}{|\nabla u|}\right)$ is the sum of the two principal curvatures of the level sets of u, (twice its mean curvature) and ν is a positive real constant. The $2D$ version of this model was heuristically justified in [5, 29]. It contains:

- A smoothing term: Twice the mean curvature in the case of (1). More efficient smoothing velocities as those proposed in [3, 9, 33, 25, 27] can be used instead of H[1].
- A constant balloon-type force similar to [12]; $\nu|\nabla u|$.
- A stopping factor $g(I)$. (Related edge detectors can be used, e.g. [47].) Note that in this model, g must be zero for the surface to stop (see next section).

[1] Although curvature flows smooth $2D$ curves [17, 18, 37, 38], a $3D$ geometric flow that smoothes all possible surfaces was not found [33]. Frequently used are mean curvature or the positive part of the Gaussian curvature flows [3, 9].

The sign conventions here are adapted to active contours propagating inwards. For active contours evolving from the inside outwards, we take $\nu < 0$. This is a drawback of this model: the active contours cannot go in both directions (see also [43]). Moreover, we always need to select $\nu \neq 0$ even if the surface is close to the object's boundary.

The goal in [7, 8] was to define a $3D$ geometric model (with level-set formulation) corresponding to the minimization of a meaningful and intrinsic energy functional. It is motivated by the extension of $2D$ geometric model to the geodesic active contours as done in [6] and briefly described in the following section.

3. Weighted minimal surfaces

In [6], a model for $2D$ object detection based on the computation of geodesics in a given Riemannian space was presented. This means that we are computing paths or curves of minimal (weighted) length. That model also shows the exact mathematical relation between energy-based active contours and those based on curvature motion, improving on those approaches. This idea may be extended to $3D$ surfaces [7, 8], computing surfaces of minimal area, where the area is defined in a given Riemannian space. In the case of surfaces, arc-length is replaced by surface area $A = \int\int da$, and weighted arc-length by "weighted" area,

$$A_R = \int\int g(I) da, \tag{2}$$

where da is the (Euclidean) element of area. Surfaces minimizing A are denoted as *minimal surfaces* [35]. In the same manner, we will denote by minimal surfaces those surfaces that minimize (2). The area element da is given by the classical area element in Euclidean space, while the area element da_r is given by $g(I)da$. Observe that da_r corresponds to the area element induced on a surface of R^3 by the metric of R^3 given by $g_{ij}\, dx_i dx_j$ with $g_{ij} = g(I)^2 \delta_{ij}$. This is the $3D$ analogue of the metric used in [6] to construct the geodesic active contour model. The energy A_R can be formally derived from the original energy formulation using basic principles of dynamical systems [6, 7, 8], further justifying this model. The basic element of the deformable model will be given by minimizing (2) by means of an evolution equation obtained from its Euler-Lagrange. Let us point out the basic characteristics of this flow.

The Euler-Lagrange of A is given by the mean curvature H, resulting a curvature (steepest descent) flow $\frac{\partial \mathcal{S}}{\partial t} = H\vec{\mathcal{N}}$, where $\mathcal{S}$ is the $3D$ surface and $\vec{\mathcal{N}}$ its inner unit normal. With the sign conventions explained above, the corresponding level-set [34] formulation is $u_t = |\nabla u| \mathrm{div}\left(\frac{\nabla u}{|\nabla u|}\right) = |\nabla u| H$. Therefore, the mean curvature motion provides a flow that computes (local) minimal surfaces [10]. Computing the Euler-Lagrange of A_R, we get

$$\mathcal{S}_t = (gH - \nabla g \cdot \vec{\mathcal{N}})\vec{\mathcal{N}}. \tag{3}$$

This is the basic weighted minimal surface flow. Taking a level-set representation, the steepest descent method to minimize (2), yields

$$\begin{aligned} \frac{\partial u}{\partial t} &= |\nabla u| \mathrm{div}\left(g(I)\frac{\nabla u}{|\nabla u|}\right) \\ &= g(I)|\nabla u| \mathrm{div}\left(\frac{\nabla u}{|\nabla u|}\right) + \nabla g(I) \cdot \nabla u. \end{aligned} \tag{4}$$

We note that comparing with previous geometric surface evolution approaches for $3D$ object detection, the minimal surfaces model includes a new term, $\nabla g \cdot \nabla u$. This term is fundamental for detecting boundaries with fluctuations in their gradient, since it will cause the surfaces to stop even if g is not zero. See [6, 7, 8] for details.

As in the $2D$ case, we can add a constant force to the minimization problem (minimizing volume), obtaining the general *minimal surfaces model* for object detection:

$$\frac{\partial u}{\partial t} = |\nabla u| \mathrm{div}\left(g(I)\frac{\nabla u}{|\nabla u|}\right) + \nu g(I)|\nabla u|. \tag{5}$$

This is the flow we will use for $3D$ object detection. It has the same properties and geometric characteristics as the geodesic active contours, leading to accurate numerical implementations and topology free object segmentation. The flow also holds important existence and completeness properties. Basically, there is a unique solution to the flow in the viscosity sense, and the flow converges to ideal objects [7, 8] (see also [20, 21]). It is also possible to bound the size of the gaps that can be successfully avoided by the flow [6, 8, 15].

As pointed out in the introduction, see [14, 16, 20, 21, 41, 43, 45, 46] for related approaches and [6, 7, 8, 24, 26, 27] for full comparisons.

4. The Tube method

4.1. Motivation

For a two-dimensional interface evolving in three space dimensions, the level set algorithm is at least an $O(N^3)$ method per time step, where N is the number of points in the spatial direction. One drawback of the technique stems from the expense; by embedding the

interface as the zero-level set of a higher dimensional function, a two-dimensional interface problem has been transformed into a three-dimensional problem.

The main idea of the tube method is to modify the level set method so it only affects points close to the region of interest, namely the cells where the front is located. This will save considerable computer time, since it reduces by an order of magnitude the number of points where terms must be evaluated. This is particularly beneficial in cases where there is significant computation to be made at each point, as well as simpler cases involving fronts propagating with a constant normal speed.

Our tube is constructed by choosing points that lie less than some given distance away from the curve. The resulting tube-like domain contains the zero-level set. This method was used before in [29] and described in more detail in [1]. A three dimensional version of the tube method was used in [2].

As an illustration, Figure 1 shows the initial surface for a circle in two dimensions. On the left the surface is defined on a square that contains the circle. On the right the surface is only defined in a neighborhood of the circle.

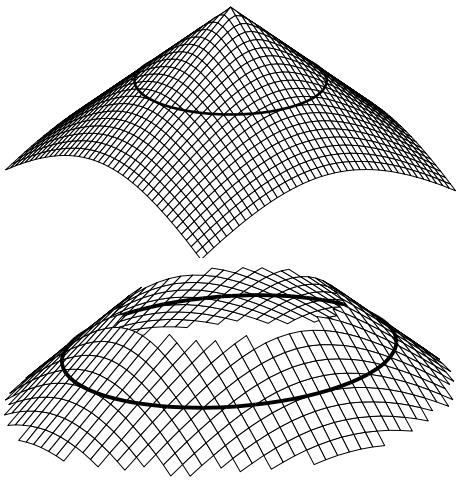

Figure 1. The signed distance function, defined on a square and a tube.

This technique saves memory usage, since all derived quantities, such as curvature and the length of the gradient require less memory than with the full method. The implementation will only store a single copy of the full array. Through careful programming, this too can be eliminated, but at the cost of considerable programming complexity.

4.2. Implementation

The definition of a tube used here is just a set of points inside a rectangular array. There are no restrictions about the shape of the tube, however most of the time it looks like a border around the current front. Initially the surface is defined as the signed distance from the front for all points closer then some predefined maximum value. Outside that tube the surface is constant, chosen to make the surface continuous on all of space.

The front is then moved the same way as in the standard level set method, however only those points belonging to the tube are updated. The tube is rebuilt whenever the front gets too close to an edge. Boundary conditions assume fixed values of u at the tube edge; a more sophisticated implementation is given in [1].

4.3. Speed comparison

To check the speed of the algorithm. we studied the collapse of a sphere with unit speed and according to its curvature. Collapse under mean curvature involves more computation than just the gradient, and better reflects the abilities of the narrow band method. Furthermore, inclusion of such parabolic terms requires smaller time steps than those required by the advection term. The initial sphere is chosen so that it almost fills the computational box. We perform timings with several different time steps and compare the execution time. The full-matrix method and the tube method require approximately the same time when there are 60 cells per side; however, as the number of grid points increases, the narrow band method becomes significantly faster than the full matrix method. Reinitializing the function values in the tube takes up sizable fraction of time but that happens only in the starting stages. The number of reinitializations is independent of the time step, so when the time step is decreased the reinitialization cost becomes a smaller fraction of the total time. We tabulate the execution times of the full matrix and the tube methods until the sphere collapses in Table 1.

5. Experimental results

The experiments described here are based on implementing the level-set flow (4) using the narrow band method [1, 30, 24, 27] and the $3D$ segmentation results are reproduced from Malladi and Sethian [27].

The volume is computed by counting the interior voxels as one volume unit (this is straightforward from the level-sets representation), and proportionally adding the contribution of boundary voxels. Linear

Grid size	Δt=0.8h	Δt=0.1h	Δt=0.05h
The full method			
$60 \times 60 \times 60$	61s	465s	925s
$100 \times 100 \times 100$	480s	3856s	7710s
$150 \times 150 \times 150$	2570s	20500s	41100s
The tube method			
$60 \times 60 \times 60$	49s	115s	182s
$100 \times 100 \times 100$	274s	591s	930s
$150 \times 150 \times 150$	1105s	2240s	3400s

Table 1. Speed comparison between the regular full matrix method and the tube method on a Sun Sparc 10 machine.

interpolation was used in this case, but more precise interpolators can be implemented if better accuracy is needed. The surface area is computed by adding the areas of all the triangles representing the zero level-set, that are extracted from the implicit representation.

The first example presents the segmentation and volume measurement of the soft tissue in a $3D$ CT data of two thighs (see Fig. 2). The computation was done by starting from a collection of spheres inside the thighs and growing outwards thereby reconstructing the thighs and the femur. Fig. 3 presents the final segmentation result in which we can observe the outer surface of the bones and the skin. The $3D$ data is given on a grid of $128 \times 128 \times 61$ which subsequently was mapped onto a unit cube; i.e. $1 \times 1 \times 1$. The measured volume of the soft tissue is 0.268492.

In Fig. 4, the left bone of the first example is extracted by using simple region growing on the segmented thighs. The volume of the bone is measured to be 0.00844465.

In the next example, we present the segmentation results of heart chambers as the heart goes through a diastolic and systolic cycle. The time varying $3D$ MRI heart image data is given on a $256 \times 256 \times 8$ grid. In Fig. 5, we show two cross-sections from the third and sixth data set from our sequence. Again, computation is made to proceed outward from a spherical initilization in the domain. Fig. 6 presents 10 samples of the cycle of a heart beat. The measurements of the area and the volume of each of the segmented heart states are presented in the two graphs in Fig. 7.

6. Concluding remarks

In this paper we presented a complete approach for detecting, representing, and measuring $3D$ medical data, extending work reported in [36, 27]. The medical object is represented as a weighted minimal surface, following [7, 8]. This is computed from geometric measures on the image, via a fast numerical implementation of the level-set approach as in [1, 24, 27]. The high accuracy of the results of the algorithm, enable us to perform measurements like volume and surface area of the detected objects, as was shown in our experiments. Interested readers are invited to visit the web site **http://www.lbl.gov/∼malladi** for movies depicting the $3D$ simulations presented in this paper.

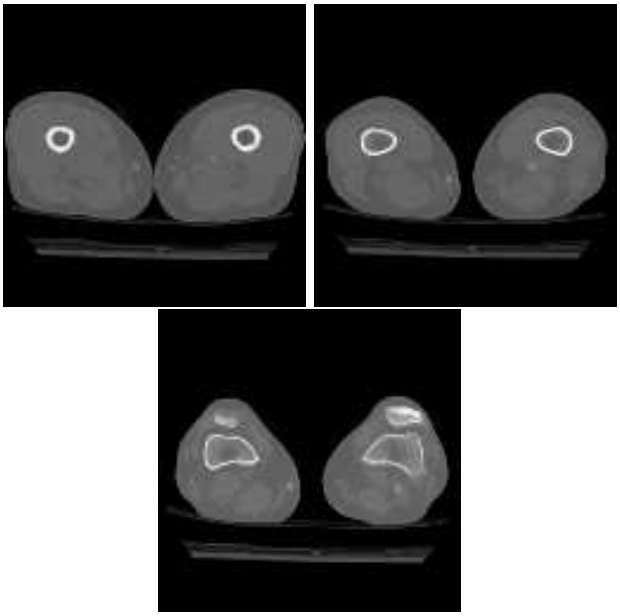

Figure 2. The 5th, 35th, and 59th cross-sections from a CT image of human thighs.

Acknowledgements

The research of RM, RK, DA, and JAS are supported in part by the Applied Mathematical Sciences Subprogram of the Office of Energy Research, U.S. Dept. of Energy under Contract DE-AC03-76SD00098. All calculations shown here were performed at University of California at Berkeley and the Lawrence Berkeley National Laboratory.

References

[1] D. Adalsteinsson and J. A. Sethian, "A fast level set method for propagating interfaces," *J. of Comp. Phys.*, **118**:269–277, 1995.

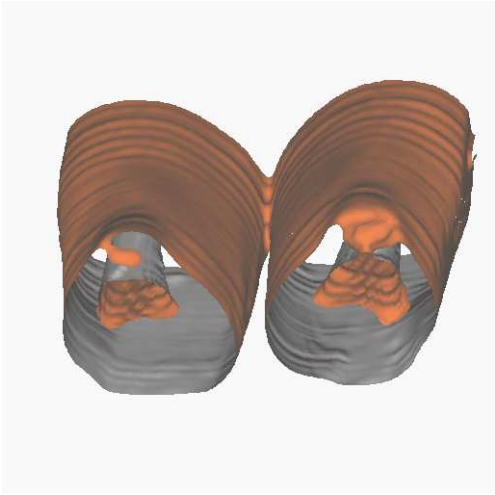

Figure 3. Detection of thighs in $128 \times 128 \times 61$ CT data images. The volume of the soft tissue was measured to be 0.268492.

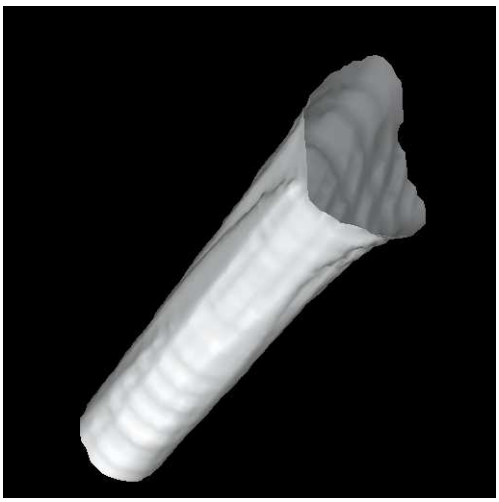

Figure 4. The left thigh bone of Fig. 3, is extracted and its volume is 0.00844465.

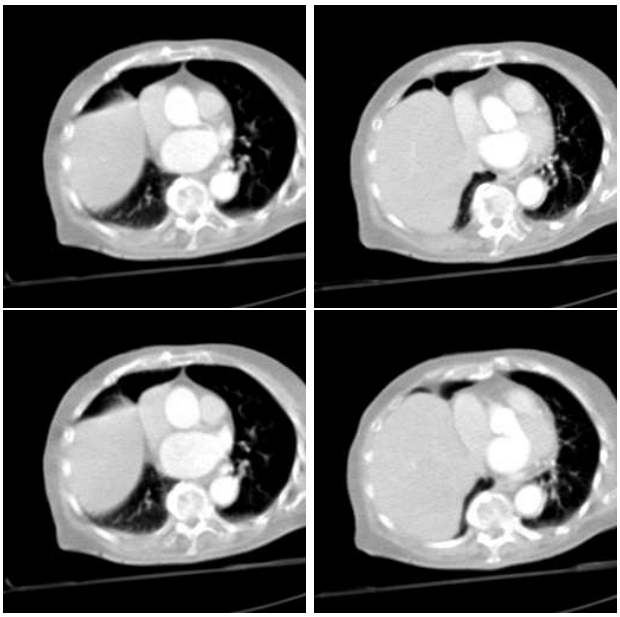

Figure 5. Two cross-sections each from third and sixth heart MRI data set.

[2] D. Adalsteinsson and J. A. Sethian, "A level-set approach to a unified model for etching, deposition, and Lithography II: Three dimensional simulations," *Journal of Comp. Phy.*, Vol. 120, pp. 128-144, 1995.

[3] L. Alvarez, F. Guichard, P. L. Lions, and J. M. Morel, "Axioms and fundamental equations of image processing," *Arch. Rational Mechanics* **123**, 1993.

[4] A. Blake and A. Zisserman, *Visual Reconstruction*, MIT Press, Cambridge, 1987.

[5] V. Caselles, F. Catte, T. Coll, F. Dibos, "A geometric model for active contours," *Numerische Mathematik* **66**, pp. 1-31, 1993.

[6] V. Caselles, R. Kimmel, and G. Sapiro, "Geodesic active contours," to appear *International Journal of Computer Vision*. A short version appears at *ICCV'95*, Cambridge, June 1995.

[7] V. Caselles, R. Kimmel, G. Sapiro and C. Sbert, "Minimal surfaces: A three-dimensional segmentation approach," *Technion Technical Report* **973**, June 1995.

[8] V. Caselles, R. Kimmel, G. Sapiro, and C. Sbert, "Three-dimensional object modeling via minimal

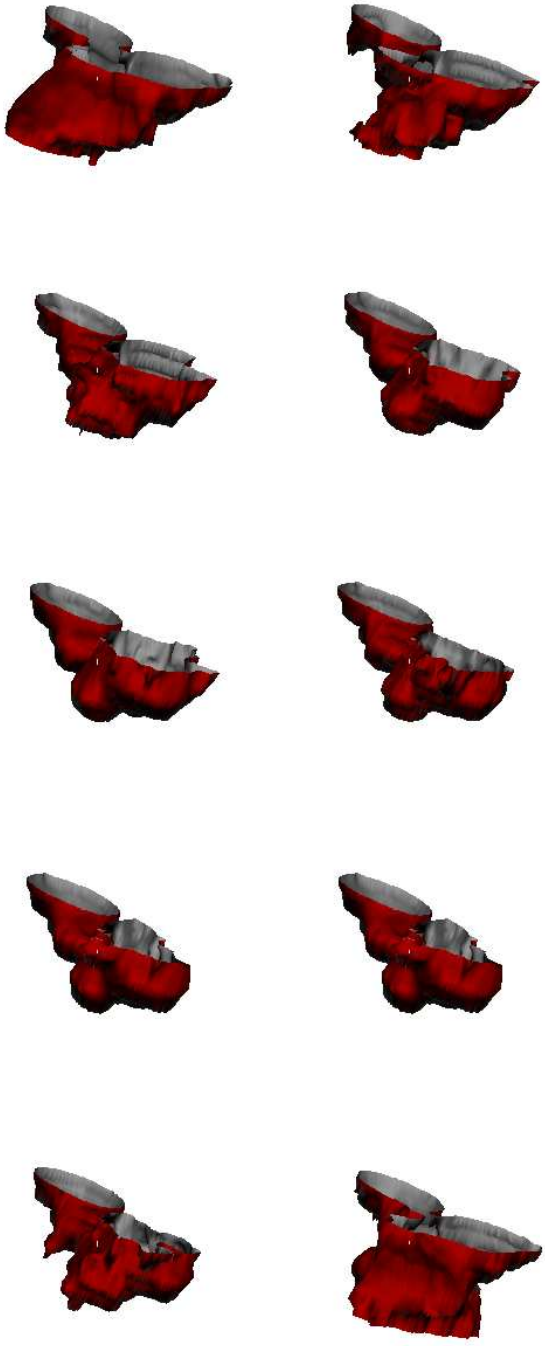

Figure 6. 10 stages along one heart beat, $3D$ segmentation results, presented left to right top to bottom.

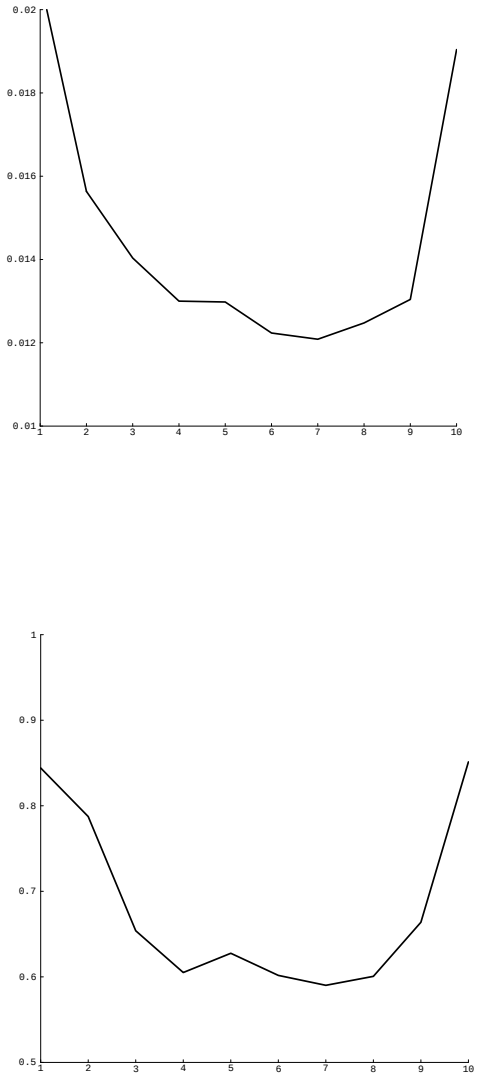

Figure 7. Volume and area (upper and lower graphs) along the heart beat cycle in Fig. 6.

surfaces." *Proc. European Conference on Computer Vision*, Cambridge-UK, April 1996.

[9] V. Caselles and C. Sbert, "What is the best causal scale-space for 3D images?," *SIAM J. on Applied Math,* to appear.

[10] D. Chopp, "Computing minimal surfaces via level set curvature flows," *J. of Comp. Phys.*, 106(1):77–91, 1993.

[11] P. Cinquin, "Un modele pour la representation d'images medicales 3d," *Proc. Euromedicine, Sauramps Medical*, **86**, pp 57-61, 1986.

[12] L. D. Cohen, "On active contour models and balloons," *CVGIP: Image Understanding* **53**, pp. 211-218, 1991.

[13] I. Cohen, L. D. Cohen, and N. Ayache, "Using deformable surfaces to segment 3D images and infer differential structure," *CVGIP: Image Understanding* **56**, pp. 242-263, 1992.

[14] L. D. Cohen and I. Cohen, "Finite element methods for active contour models and balloons for 2D and 3D images," *IEEE Tran. on PAMI* **15**(11), November, 1993.

[15] L. D. Cohen, and R. Kimmel, "Global minimum for active contour models: A minimal path approach," submitted to *IJCV*, 1996; to appear *Proc. CVPR*, June 1996.

[16] P. Fua and Y. G. Leclerc, "Model driven edge detection," *Machine Vision and Applications,* **3**, pp. 45-56, 1990.

[17] M. Gage and R. S. Hamilton, "The heat equation shrinking convex plane curves," *J. Differential Geometry* **23**, pp. 69-96, 1986.

[18] M. Grayson, "The heat equation shrinks embedded plane curves to round points," *J. Differential Geometry* **26**, pp. 285-314, 1987.

[19] M. Kass, A. Witkin, and D. Terzopoulos, "Snakes: Active contour models," *International Journal of Computer Vision* **1**, pp. 321-331, 1988.

[20] S. Kichenassamy, A. Kumar, P.Olver, A. Tannenbaum, and A. Yezzi, "Gradient flows and geometric active contour models," *Proc. ICCV*, Cambridge, June 1995.

[21] S. Kichenassamy, A. Kumar, P.Olver, A. Tannenbaum, and A. Yezzi, "Conformal curvature flows: from phase transitions to active vision," to appear *Archive for Rational Mechanics and Analysis.*

[22] B. B. Kimia, A. Tannenbaum, and S. W. Zucker, "Shapes, shocks, and deformations, I," *International Journal of Computer Vision* **15**, pp. 189-224, 1995.

[23] R. Kimmel, "Curve evolution on surfaces," D. Sc. Thesis, Technion, Israel, June 1995.

[24] R. Malladi, D. Adalsteinsson, and J. A. Sethian, "Fast method for 3D shape modeling using level sets," submitted.

[25] R. Malladi and J. A. Sethian, "Image processing: Flows under min/max curvature and mean curvature," *Graphical Models and Image Processing*, Vol. 58(2), pp. 127–141, March 1996.

[26] R. Malladi and J. A. Sethian, "A unified approach to noise removal, image enhancement, and shape recovery," *IEEE Trans. Image Processing*, to appear, November 1996.

[27] R. Malladi and J. A. Sethian, "Fast level set methods for curvature flow, minimal surfaces, image processing and shape recovery," *Proc. of International Conference on Visualization and Mathematics*, Ed. K. Polthier, Berlin, June 1995, in press, Springer-Verlag.

[28] R. Malladi, J. A. Sethian and B. C. Vemuri, "Evolutionary fronts for topology independent shape modeling and recovery," *Proc. of the 3rd ECCV*, Stockholm, Sweden, pp. 3-13, 1994.

[29] R. Malladi, J. A. Sethian and B. C. Vemuri, "Shape modeling with front propagation: A level set approach," *IEEE Trans. on PAMI,* Vol. 17(2), pp. 158-175, Feb. 1995.

[30] R. Malladi, J. A. Sethian and B. C. Vemuri, "A fast level set based algorithm for topology independent shape modeling," *Journal of Mathematical Imaging and Vision*, Special Issue on Topology and Geometry in Computer Vision, Ed. A. Rosenfeld and Y. Kong, Vol. 6: 2/3, pp. 269–290, April 1996.

[31] T. McInerney and D. Terzopoulos, "Topologically adaptable snakes," *Proc. ICCV*, Cambridge, June 1995.

[32] D. Mumford and J. Shah, "Optimal approximations by piecewise smooth functions and variational problems," *Comm. Pure and App. Math.* **42**, 1989.

[33] P. J. Olver, G. Sapiro, and A. Tannenbaum, "Invariant geometric evolutions of surfaces and volumetric smoothing," *SIAM J. of Appl. Math.*, to appear.

[34] S. J. Osher and J. A. Sethian, "Fronts propagation with curvature dependent speed: Algorithms based on Hamilton-Jacobi formulations," *Journal of Computational Physics* **79**, pp. 12-49, 1988.

[35] R. Osserman, *Survey of Minimal Surfaces*, Dover, 1986.

[36] G. Sapiro, R. Kimmel, and V. Caselles, "Object detection and measurements in medical images via geodesic active contours," *Proc. SPIE-Vision Geometry*, San Diego, July 1995.

[37] G. Sapiro and A. Tannenbaum, "On affine plane curve evolution," *Journal of Functional Analysis* **119:1**, pp. 79-120, 1994.

[38] G. Sapiro and A. Tannenbaum, "Affine invariant scale-space," *International Journal of Computer Vision* **11:1**, pp. 25-44, 1993.

[39] J. A. Sethian, "A review of recent numerical algorithms for hypersurfaces moving with curvature dependent flows," *J. Differential Geometry* **31**, pp. 131-161, 1989.S

[40] J. A. Sethian, "A Review of the Theory, Algorithms, and Applications of Level Set Methods for Propagating Interfaces," in press, Acta Numerica, 1995.

[41] J. Shah, "Recovery of shapes by evolution of zero-crossings," Technical Report, Math. Dept. Northeastern Univ. Boston MA, 1995.

[42] R. Szeliski, D. Tonnesen, and D. Terzopoulos, "Modeling surfaces of arbitrary topology with dynamic particles," *Proc. CVPR*, pp. 82-87, 1993.

[43] H. Tek and B. B. Kimia, "Image segmentation by reaction-diffusion bubbles," *Proc. ICCV*, Cambridge, June 1995.

[44] D. Terzopoulos, A. Witkin, and M. Kass, "Constraints on deformable models: Recovering 3D shape and nonrigid motions," *Artificial Intelligence* **36**, pp. 91-123, 1988.

[45] R. T. Whitaker, "Volumetric deformable models: Active blobs," *Visualization in Biomedical Computing*, pp. 122–134, 1994.

[46] R. T. Whitaker, "Algorithms for implicit deformable models," *Proc. ICCV'95*, pp. 822–827, Cambridge, June 1995.

[47] S. W. Zucker and R. A. Hummel, "A three-dimensional edge operator," *IEEE-PAMI* **3**, pp. 324-331, 1981.